RESEARCH

Androgen deprivation therapy promotes an obesity-like microenvironment in periprostatic fat

Stefano Mangiola[1,2,3], Ryan Stuchbery[2], Patrick McCoy[2,3], Ken Chow[2,3], Natalie Kurganovs[2,4,5,6], Michael Kerger[4], Anthony Papenfuss[1,7,8,9,10], Christopher M Hovens[2,3] and **Niall M Corcoran[2,3,11]**

[1]Bioinformatics Division, Walter and Eliza Hall Institute, Parkville, Victoria, Australia
[2]Department of Surgery, The University of Melbourne, Parkville, Victoria, Australia
[3]Department of Urology, Royal Melbourne Hospital, Parkville, Victoria, Australia
[4]Australian Prostate Cancer Research Centre Epworth, Richmond, Victoria, Australia
[5]Ontario Institute for Cancer Research, Toronto, Canada
[6]Princess Margaret Cancer Centre, University Health Network, Toronto, Canada
[7]Peter MacCallum Cancer Centre, Melbourne, Victoria, Australia
[8]Department of Medical Biology, University of Melbourne, Melbourne, Victoria, Australia
[9]Sir Peter MacCallum Department of Oncology, University of Melbourne, Melbourne, Victoria, Australia
[10]Department of Mathematics and Statistics, University of Melbourne, Melbourne, Victoria, Australia
[11]Department of Urology, Frankston Hospital, Frankston, Victoria, Australia

Correspondence should be addressed to N M Corcoran: niallmcorcoran@gmail.com

Abstract

Prostate cancer is a leading cause of morbidity and cancer-related death worldwide. Androgen deprivation therapy (ADT) is the cornerstone of management for advanced disease. The use of these therapies is associated with multiple side effects, including metabolic syndrome and truncal obesity. At the same time, obesity has been associated with both prostate cancer development and disease progression, linked to its effects on chronic inflammation at a tissue level. The connection between ADT, obesity, inflammation and prostate cancer progression is well established in clinical settings; however, an understanding of the changes in adipose tissue at the molecular level induced by castration therapies is missing. Here, we investigated the transcriptional changes in periprostatic fat tissue induced by profound ADT in a group of patients with high-risk tumours compared to a matching untreated cohort. We find that the deprivation of androgen is associated with a pro-inflammatory and obesity-like adipose tissue microenvironment. This study suggests that the beneficial effect of therapies based on androgen deprivation may be partially counteracted by metabolic and inflammatory side effects in the adipose tissue surrounding the prostate.

Key Words

- prostate
- cancer
- obesity
- adipose tissue
- transcriptomics
- transcriptomic econvolution

Endocrine Connections (2019) **8**, 547–558

Introduction

For over 80 years, androgen deprivation by surgical or medical castration has been the cornerstone of treatment for advanced prostate cancer (1). As new cytotoxic and androgen receptor-targeted therapies have been developed, demonstrating survival benefit in combination with androgen deprivation in a number of clinical settings, the duration a patient can expect to be in a castrated state prior to death has been extended significantly (2). Given that androgen signalling is important for homeostasis in a number of different organ systems, it is not surprising that both short- and long-term use is associated with a number of deleterious effects (3).

Forefront of these is the association of androgen deprivation with metabolic syndromes such as diabetes

https://ec.bioscientifica.com
https://doi.org/10.1530/EC-19-0029

mellitus (4) and obesity (5), as androgens play a key role in the regulation of intermediate metabolism and tissue composition (6). Increased fat tissue mass (known in conjunction with loss of muscle mass as sarcopenic obesity) is one of the main metabolic side effects of androgen deprivation therapy (ADT) (7), even for short-term treatment (8, 9, 10). At the molecular level, lack of androgen-related hormones leads to changes in tissue lipid composition and decreased insulin sensitivity (4). For example, gonadotropin-releasing hormone agonists have been shown to alter tissue lipid profiles with cholesterol levels, triglycerides and high-density lipoproteins shown to increase up to 10.6, 25 and 8–20%, respectively (8, 10).

The promotion of an obese-like phenotype by androgen deprivation is highly clinically relevant, as obesity (expressed as BMI) is itself associated with the development of prostate cancer, post-prostatectomy biochemical failure and risk of death from prostate cancer. Although the link between elevated BMI and increased risk of prostate cancer is still controversial (11, 12, 13), several studies have found a positive association between BMI and cancer grade and/or stage at the time of radical prostatectomy (14, 15, 16). Two recent studies identified an association between BMI and biochemical failure rates following radical prostatectomy, based on a large-scale, multi-ethnic cohort (13, 17). The relationship between BMI and prostate cancer-specific mortality is also widely supported (18, 19, 20, 21).

Although the connection between ADT, obesity and prostate cancer progression is well established in clinical settings, a molecular understanding of the changes in adipose tissue associated with castrating therapies is still missing, in part due to a paucity of appropriate clinical specimens. This is especially important for periprostatic adipose tissue due to its proximity to the cancer site and its potential to influence prostate hormonal and immune homeostasis (22). Here for the first time, based on a unique cohort of patients with 6-month profound androgen suppression and receptor blockade, we performed an integrative study of the molecular and cellular changes in periprostatic fat associated with androgen deprivation. In this study, we show that ADT is associated with a pro-inflammatory and obesity-like adipose tissue microenvironment.

Materials and methods

Ethics statement

The collection and use of tissue for this study had Epworth Healthcare institutional review board approval and patients provided written informed consent (HREC approval number 34506).

Study cohort selection

ADT-treated patients ($n=11$) were recruited from an open-label neoadjuvant phase II study in which patients with high-risk disease received a 'supercastration' regimen consisting of degarelix 240/80 mg subcutaneously every 4 weeks; abiraterone acetate 500 mg orally daily titrating upwards every 2 weeks by 250 mg to a final dose of 1000 mg daily; bicalutamide 50 mg orally daily and prednisolone 5 mg orally twice daily for a total of 6 months (Australian New Zealand Clinical Trials Registry 12612000772842). Untreated patients with similar pre-treatment characteristics were obtained from a prospective prostatectomy biorepository (22, 23). Prior to ligation of the dorsal venous complex and prostate pedicles, the anterior prostate was defatted and the specimen was removed immediately, placed in a sterile container and transferred on ice for long-term storage in the vapour phase of liquid nitrogen. Patients were risk categorised using the CAPRA scoring system, which uses pre-treatment clinical and pathological variables (including age, serum PSA level, biopsy tumour grade, clinical stage) to predict the risk of bone metastasis and prostate cancer-specific mortality (24). Differences between patient groups were assessed by the Mann–Whitney or chi-squared test as appropriate.

Gene expression screen

A total of 50–100 µg of adipose tissue was separated from fresh frozen samples stored at −160°C. RNA was isolated using the Qiagen RNeasy Lipid Tissue Mini Kit and eluted in 35 µL nuclease-free water. 0.5–1 µg of total RNA was used as the input for cDNA library synthesis using TruSeq RNA Sample Prep Kit v2 (Illumina), and libraries were constructed according to manufacturer's instructions. Samples were sequenced on a HiSeq 2500 (Illumina) using 101 base paired-end chemistry, aiming for 50 million mapped paired-end reads per sample.

Data pre-processing and mapping

The RNA-sequencing quality for each sample was controlled using the FastQC algorithm (25). Reads were trimmed for Illumina adapters and low-quality fragments using the Trimmomatic algorithm, and short reads filtered out from the pools according to default settings (26).

https://ec.bioscientifica.com
https://doi.org/10.1530/EC-19-0029

The remaining reads were aligned to the reference genome (hg19) with the STAR aligner using default settings (27). The gene abundance for each sample was quantified in terms of reads per gene (read-count) using featureCounts (28). Low abundance genes were filtered from the analysis, if not present in at least 0.5 parts per million in two-thirds of the samples in each treatment group (i.e., treated and naïve).

Differential expression and gene set enrichment analyses

Considering the sparse batch distribution, the gene abundances were adjusted for unknown variation using RUVseq with one unwanted covariate (using default settings) (29). The resulting covariate matrix for the unwanted covariate was appended to the design matrix (i.e. treated vs naïve, plus the intercept term); then, all samples were tested for differential transcription using the edgeR package (30), considering differentially transcribed genes with a false discovery rate <0.05. Ensemble pathway analyses were performed using the algorithm EGSEA (31). In order to test for the enrichment of an obesity molecular phenotype among the differentially transcribed genes, an *ad hoc* signature data set (46) was queried using the algorithm GSEA (32).

Differential tissue composition analyses

The associations between (i) the abundance of stromal and immune cell types within the tissue and (ii) the treatment status (i.e., treated or naïve) was inferred using two distinct approaches. Both approaches included a two-step inference, where the cellular composition of each sample is inferred first (i.e., the proportion of several cell types within the tissue sample), and an association analysis is performed integrating such inference with the treatment status. The first approach applied the algorithm Cibersort (33), for the inference of tissue composition, in combination with DirichletReg (34), for the regression of the proportional estimates produced by Cibersort. Considering that Cibersort was designed mainly for microarray data, and only for PBMC cell types, a custom probabilistic Bayesian model was also implemented (Fig. 1) based on the Markov chain Monte Carlo probabilistic framework Stan (35), which natively models RNA sequencing data and performs association analysis in an integrative manner preserving uncertainty information between the two steps. This probabilistic model can be described by a joint probability density formula and a series of sampling statements (Supplementary Figure 1, see section on supplementary data given at the end of this article).

qRT-PCR validation

In order to validate the methodology used for the inference of differential transcription, qRT-PCR was used for an independent observation of gene transcript abundance. A total of nine differentially transcribed genes were selected for validation with qRT-PCR, based on false discovery rate (<0.05), log fold change (>2) and on the absence of clear outliers. The qRT-PCR validation was performed using 1 µL of cDNA, 0.5 µL qRT-PCR primers (see below), 5 µL of

$$(1)\ P(\sigma)\,P(\phi)\,P(\delta)\prod_{r=1}^{R}\prod_{p=1}^{P}P(\alpha_{r,p}|\delta)\prod_{p=1}^{P}\prod_{s=1}^{S}P(\pi_{p,s}|X_s,\alpha_p,\phi)\prod_{s=1}^{S}\prod_{g=1}^{G}P(Y_{s,g}|x_g,\pi_s,\sigma_s,\theta^*)$$

$$(1)\ P(Y|x,\pi,\sigma,\theta^*)\sim lognormal(x*\pi,\sigma)$$

$$(2)\ P(\pi|X,\alpha,\phi)\sim Dirichlet(\widehat{\widehat{Y}})$$

$$(3)\ P(\alpha|\delta)\sim Dirichlet\left(\left[\delta_1,...,\delta_k\right]\right)$$

$$(4)\ P(\sigma)\sim normal(0,0.1)$$

$$(5)\ P(\phi)\sim normal(1,...)$$

$$(6)\ P(\delta)\sim cauchy(1,2)$$

$$(7)\ \widehat{\widehat{Y}}=softmax(\widehat{Y})*\sigma$$

$$(8)\ \widehat{Y}=X\cdot\alpha$$

$$(9)\ \mathrm{softmax(z)}_j=\frac{e^{z_j}}{\sum_{k=1}^{K}e^{z_k}}for j=1,...,K$$

Figure 1
Probabilistic Bayesian inference model. The parameter α represents the rates of change of each cell type category along the biological conditions. The parameter π represents the matrix of proportions for each cell type category and sample. The parameters σ, φ and δ define the noise model. The point estimate and credible intervals for both cell type proportions and trends of change are calculated from the posterior distribution.

https://ec.bioscientifica.com
https://doi.org/10.1530/EC-19-0029

TaqMan Fast Advanced Master Mix (Applied Biosystems) and 3.5 µL of UltraPure distilled water (Gibco). The primers, including *ART3* (Hs00922621_m1), *CSDC2* (Hs00411093_m1), *DIO*$_2$ (Hs05050546_s1), *FCGR1B* (Hs00174081_m1), *LYZ* (Hs00426232_m1), *OR51E2* (Hs00258239_s1), *SLC16A12* (Hs01584854_m1), *SUSD5* (Hs01394532_m1), and *TRIM67* (Hs01595609_m1), were pre-designed and commercially available from Applied Biosystems. Samples were run on a 384-well plate using a Viia7 qRT-PCR machine (Applied Biosystems) under the following conditions: UNG incubation at 50°C for 2 min; polymerase activation at 95°C for 20 s; followed by 40 cycles of denaturation at 95°C for 1 s; anneal/extend at 60°C for 20 s. Expression levels of target genes were normalised to the geometric mean of *GAPDH* (Hs00266705_g1, Applied Biosystems), *TBP* (Hs00427621_m1, Applied Biosystems) and *POLR2A* (Hs00427621_m1, Applied Biosystems) using the formula $2^{-\Delta C(T)}$. One-sided Student's *t*-test was used for hypothesis testing; then, Bonferroni multiple-test correction was applied to the produced *P* values.

Results and discussion

Patient characteristics

The treated and naïve groups comprised 11 and 10 patients respectively; their clinical and pathological characteristics are shown in Table 1. Given that pre-operative risk assessment is frequently inaccurate (36, 37), being biased towards underestimation of tumour grade and stage, patients in the high-risk cohort were selected based on the stage, grade and volume of tumour in the prostatectomy specimen. All patients in the treated cohort had high-risk disease at the time of initial assessment, although the ultimate response to androgen deprivation was highly variable. On average, patients exposed to androgen suppression experienced a 3.3% increase in body weight/BMI from baseline over the course of treatment.

Differentially transcribed genes represent three main functional groups

The RNA sequencing libraries had an average of 55 million reads across the 21 samples. All samples had a Phred quality score exceeding 28 following filtering and trimming (25). As expected, the distribution of the multidimensional scaling (MDS) analysis (38) including both treated and naïve groups showed the improvement in clustering obtained through the removal of unwanted variation (RUVseq; Fig. 2A and B). However, the overall magnitude of differences between the two groups was low (i.e., log fold difference <3; Fig. 2B and C). No significant difference was found between the two treatment categories for BMI or CAPRA-S risk score distributions (adjusted *P* value = 1.0 and 1.0 respectively; Supplementary Fig. 1).

A total of 70 genes were identified as differentially transcribed (false discovery rate <0.05; Supplementary Table 1), characterised by a median fold change of 3.23. Of these, 49 genes were characterised by a fold change greater than 2. Among the differentially transcribed genes with fold change greater than 2, three recurring biological processes (from grouping analogous gene ontology annotations; GO (39); Supplementary Table 2) were identified: hormonal and fat homeostasis ($n=8$), inflammation ($n=8$) and neural plasticity ($n=4$) (Fig. 2D). Several genes involved in cholesterol metabolism were

Table 1 Clinical characteristics of study cohort.

	Naïve	Treated	*P* value
Age (years)			
Median	66	65	0.79
Range	49–72	63–72	
PSA (ng/dL)			
Median	7.5	14.4	0.46
Range	2.7–27	4.4–95	
<10	7	5	0.35
10–20	2	2	
>20	1	4	
Clinical Stage			
cT1	3	2	0.08
cT2	7	4	
cT3	0	5	
Biopsy grade			
ISUP2	2	1	0.16
ISUP3	3	0	
ISUP4	2	3	
ISUP5	3	7	
Pathological stage			
pT0	0	1	0.13
pT2	0	3	
pT3	10	8	
Prostatectomy grade			
ND	0	1	0.26
ISUP1	0	2	
ISUP2	0	1	
ISUP3	3	1	
ISUP4	1	2	
ISUP5	6	5	
Tumour volume			
Median	7.1	1	0.012
Range	0.7-17.8	0-9.3	
BMI (kg/m^2)			
Mean	26.9	28.2	0.67
S.D.	2.9	4	

BMI, body mass index; PSA, prostate-specific antigen.

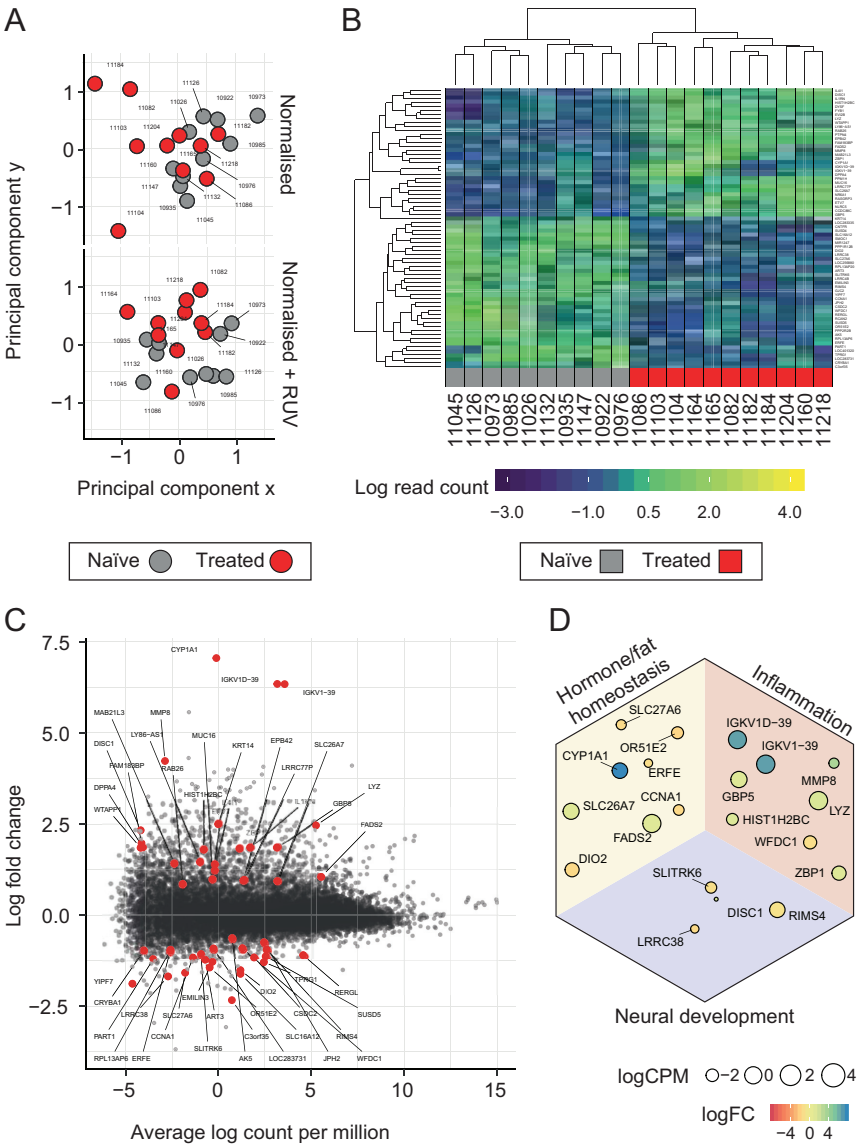

Figure 2
(A) Heatmap of the top differentially regulated genes, with unsupervised hierarchical clustering for samples and genes. (B) Multidimensional scaling (MDS) plot of the treated and naïve cohorts before and after removal of the unwanted variation (K = 1). (C) Smear plot indicating the differentially transcribed genes in red. (D) Recurrent functional groups within the differentially transcribed genes.

found to be upregulated from the hormonal homeostasis gene set. One such gene encodes for cytochrome P450, family 1, member A1 (*CYP1A1*), which catalyses several reactions involved in the synthesis of cholesterol, steroids and other lipids, as well as drug metabolism (40). Another upregulated gene, fatty acid desaturase 2 (*FADS2*), is a known modulator of lipid composition in skin (41). Within the treated cohort, several genes were decreased in abundance such as iodothyronine deiodinase 2 (*DIO2*), which is associated with the biosynthesis of thyroid hormone (42) and cyclin A1 (*CCNA1*), which is involved in spermatogenesis (43). For inflammation, upregulated genes were enriched over downregulated genes ($n=7$ vs 1 respectively). The transcriptional changes with larger magnitude involved two paralog genes (i.e., *IGKV1D–39* and *IGKV1–39*) encoding for 'v' region of the variable domain of immunoglobulin light chains, mainly secreted by B lymphocytes and participating in antigen recognition (44). The only downregulated gene within the inflammation category was WAP four-disulfide core domain 1 (*WFDC1*), which is linked to negative regulation of the inflammatory response (45).

For neural development, the transcript abundance of most genes was decreased in treated patients, including several genes regulating synapse formation such as regulating synaptic membrane exocytosis 4 (*RIMS4*). Among nine differentially transcribed genes, a total of seven validated with qRT-PCR, after correcting for multiple hypothesis testing (i.e. adjusted P value <0.05; Supplementary Fig. 2).

https://ec.bioscientifica.com
https://doi.org/10.1530/EC-19-0029

Enriched inflammatory signature

Overall, the gene enrichment analysis performed by EGSEA showed a pro-inflammatory signature for all query data sets (e.g. Hallmarks, Gene Ontology, KEGG and Immune Signatures; Table 2) (31). The pathways within the immune signature data set included *IL6/JAK/STAT3* signalling, interferon gamma response, positive regulation of immune response and antigen processing and presentation. Specifically for the immune signature dataset, transcriptional changes pointed to the differentiation of immature immune cell types (i.e., immature dendritic cells and monocytes), as well as neutrophil and mast cell activation.

Consistent with the gene enrichment analyses, the differential tissue composition analysis based on our Bayesian inference model showed a positive association between overall immune cell abundance and treatment status (Fig. 3A). In the two approaches employed for differential tissue composition analysis, monocyte-derived cells dominated the immune population within adipose tissue across the treated and naïve cohorts. Signatures of macrophages, monocytes and granulocytes were enriched by our model within the immune cell population in treated patients compared to naïve. This inference was partially consistent with that of the Cibersort-DirichletReg approach (i.e. for monocytes and macrophages; Fig. 3B). The latter approach uniquely identified an association involving CD4 memory resting, NK cells resting and mast cells resting. Although a significant enrichment of CD8+ T-cells in treated patients was not observed using our statistical model and the Cibersort-DirichletReg approach, a positive association appears to exist when observing the distributions of the estimated cell type proportions (Supplementary Fig. 3). As expected, considering the absence of a robust adipocyte transcriptomic signature within the model, the fibroblast cell type appears to have captured the adipocyte transcriptomic profile (Supplementary Fig. 3). The differences observed in the average estimated proportions for immune cell types between Cibersort and our statistical method are in part due to the inclusion of non-immune cells (e.g. fibroblasts, endothelial and epithelial) in our model, while Cibersort models selectively estimate immune cells as composing the totality of the tissue.

Enriched obesity signature

The analysis of a previously published obesity transcriptional signature for adipose tissue (46) revealed a positive association with androgen deprivation treatment independent of BMI (false discovery rate of 8.4×10^{-3}; Fig. 4). Within the ten top ranked genes

Table 2 EGSEA results.

GeneSet	Direction	*P* value	*P* adj
Hallmark signatures			
Hallmark allograft rejection	Up	$<1.0 \times 10^{-16}$	$<1.0 \times 10^{-16}$
Hallmark kras signalling up	Up	$<1.0 \times 10^{-16}$	1.0×10^{-06}
Hallmark inflammatory response	Up	$<1.0 \times 10^{-16}$	$<1.0 \times 10^{-16}$
Hallmark IL6 jak stat3 signalling	Up	8.0×10^{-06}	5.0×10^{-05}
Hallmark interferon gamma response	Up	$<1.0 \times 10^{-16}$	$<1.0 \times 10^{-16}$
Gene ontology			
GO regulation of innate immune response	Up	2.0×10^{-06}	3.8×10^{-05}
GO innate immune response	Up	$<1.0 \times 10^{-16}$	9.0×10^{-06}
GO positive regulation of defence response	Up	4.0×10^{-06}	8.4×10^{-05}
GO positive regulation of immune response	Up	$<1.0 \times 10^{-16}$	9.0×10^{-06}
GO immune system process	Up	4.9×10^{-05}	7.1×10^{-4}
KEGG			
hsa04612 Antigen processing and presentation	Up	$<1.0 \times 10^{-16}$	$<1.0 \times 10^{-16}$
hsa05152 Tuberculosis	Up	1.7×10^{-05}	1.6×10^{-4}
hsa05164 Influenza A	Up	2.2×10^{-05}	2.0×10^{-4}
hsa05332 Graft-versus-host disease	Up	$<1.0 \times 10^{-16}$	$<1.0 \times 10^{-16}$
hsa05140 Leishmaniasis	Up	$<1.0 \times 10^{-16}$	$<1.0 \times 10^{-16}$
Immune signatures			
GSE7509 Genes downregulated in immature dendritic cells	Up	$<1.0 \times 10^{-16}$	$<1.0 \times 10^{-16}$
GSE2706 Genes downregulated in comparison of unstimulated DC	Up	$<1.0 \times 10^{-16}$	$<1.0 \times 10^{-16}$
GSE19888 Genes upregulated in HMC-1 (mast leukaemia) cells	Up	$<1.0 \times 10^{-16}$	$<1.0 \times 10^{-16}$
GSE34156 Genes downregulated in monocytes	Up	$<1.0 \times 10^{-16}$	$<1.0 \times 10^{-16}$
GSE37416 Genes upregulated in activated neutrophils	Up	7.0×10^{-06}	9.7×10^{-05}

https://ec.bioscientifica.com
https://doi.org/10.1530/EC-19-0029

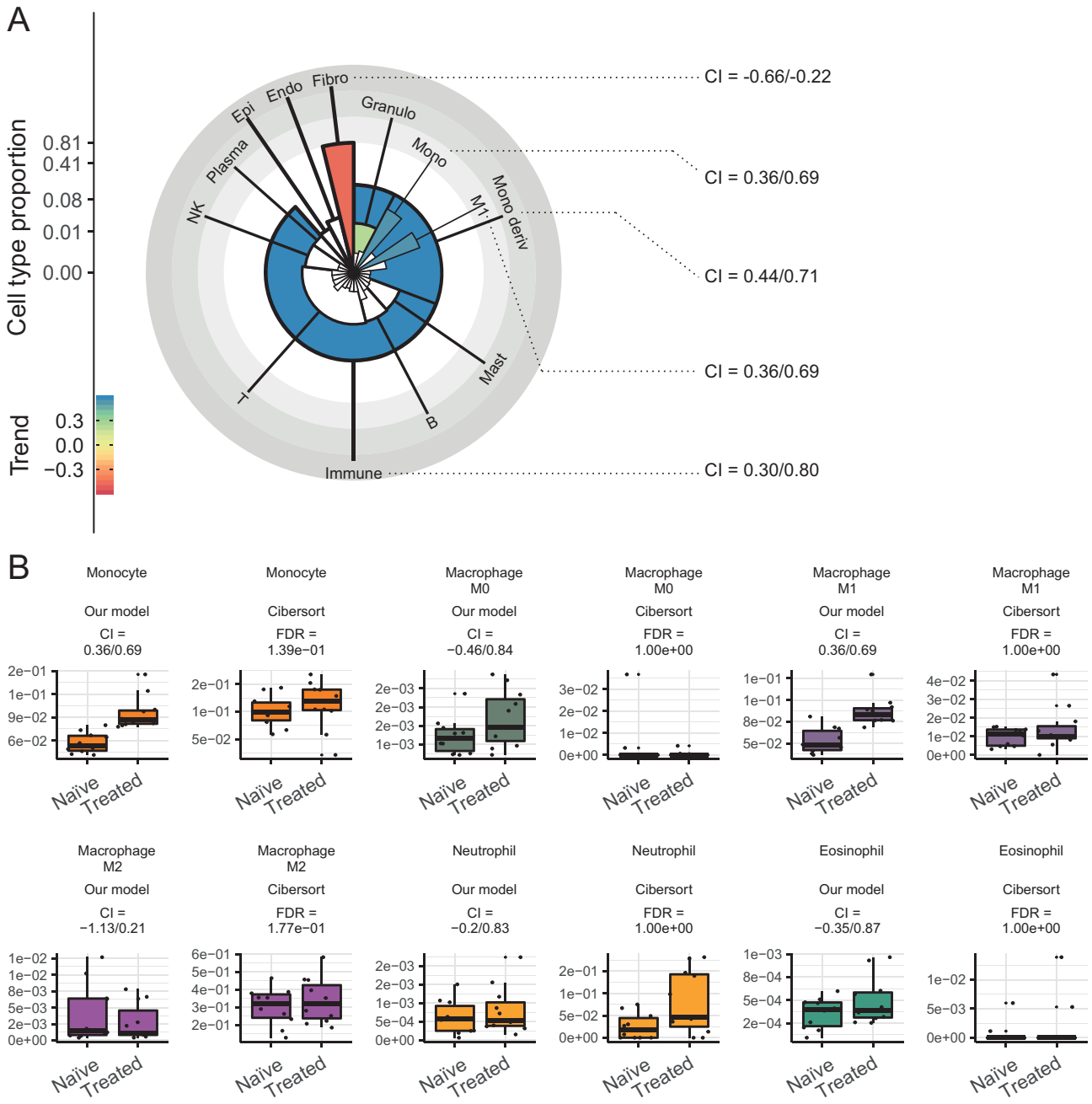

Figure 3
Differential tissue composition analysis. (A) Polar plot representing the overall cell type abundance (i.e. radius dimension) and the significant associations with androgen deprivation therapy (i.e. white for non-significant associations). Cell types are labelled if more abundant than 1%. CI = 95% credible interval of the association. (B) Boxplots of the inferred cell type proportions by our Bayesian probabilistic model and Cibersort, for the cell types that correspond or are part of significantly differentially abundant cell type categories (e.g. the differentially abundant category 'granulocytes' include eosinophils and neutrophils) between the two treatment categories (i.e., treated and naïve) according to our model. FDR = false discovery rate linked to an association being different non null.

present in the obesity signature, the majority were linked to inflammation (Supplementary Table 2), including Fc fragment of IgG-binding protein (*FCGBP*), lysozyme (*LYZ*), chemokine ligand motif 10 (*CXCL10*), myeloid cell nuclear differentiation antigen (*MNDA*), toll like receptor 8 (*TLR8*) and a member of the STAT family (*STAT1*), which is activated by various ligands including interferon alpha, interferon gamma (*IFNγ*), epidermal growth factor (*EGF*), platelet derived growth factor (PDGF) and interleukin 6 (IL6). The third top ranked gene (included in the obesity signature)

https://ec.bioscientifica.com
https://doi.org/10.1530/EC-19-0029

is a key regulator of hormonal homeostasis (*DHRS9*), which is able to convert 3-alpha-tetrahydroprogesterone to dihydroxyprogesterone and 3-alpha-androstanediol to dihydroxyprogesterone in the cytoplasm (47); also, it is a marker for regulatory macrophages (48). Regulatory genes for calcium homeostasis were also present, including S100 calcium-binding protein A1 (*S100A1*) and stanniocalcin 2 (*STC2*), which regulate renal and intestinal calcium and phosphate transport (49).

Conclusions

The prostate gland is enveloped in adipose tissue, and over the last decade a number of lines of evidence suggest that paracrine interactions between this fat depot and prostate epithelium play a role in prostate cancer development and/or progression. For instance, tumour cell invasion into the periprostatic fat compartment where direct cell-to-cell interaction can occur has been reported to be a stronger determinant of cancer recurrence than acquisition of the ability to invade across tissue boundaries (50). Periprostatic adipose tissue has been shown to elaborate a number of cytokines including IL6, osteopontin, and TNF-alpha, that promote prostate tumour cell migration and invasion (51, 52), and at least for IL6 correlates with downstream pathway activation in high-grade tumours (53). In addition, there is evidence of a positive feedback loop, with conditioned media from prostate cancer cells significantly increasing the secretion of these cytokines from adipose tissue explants (52).

The role of adipose tissue in prostate cancer progression is perhaps best understood in the context of obesity, where numerous clinical studies report positive associations between BMI and high-risk pathological findings at prostatectomy as well as adverse clinical outcomes post treatment (54). Obesity induces a persistent inflammatory and hormone-rich tissue microenvironment that contributes to high-risk disease (55, 56). ADT is a known cause of increased fat body mass (14, 15, 16); yet, the cellular and molecular processes that are altered in association with ADT, especially in the periprostatic adipose tissue microenvironment, have not been completely resolved. In this study, we showed that profound ADT is associated with a pro-inflammatory adipose tissue microenvironment, as well

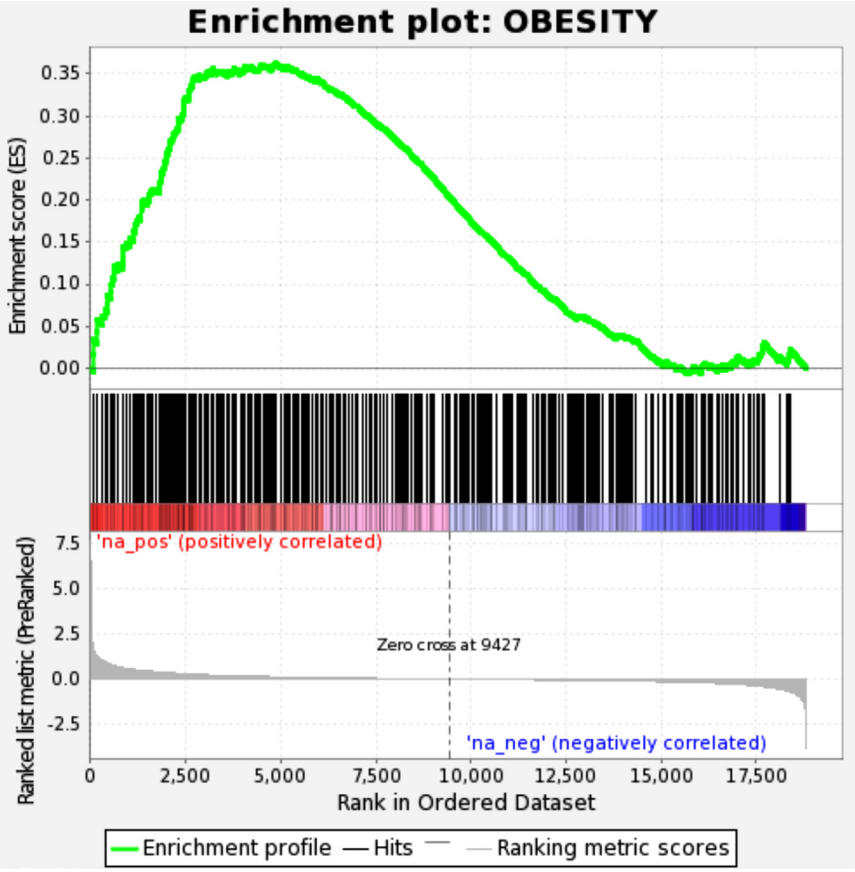

Figure 4
GSEA enrichment plot showing the significant enrichment of the obesity signature among the most differentially transcribed genes.

https://ec.bioscientifica.com
https://doi.org/10.1530/EC-19-0029

as with altered obesity-related gene transcription linked with cholesterol and hormonal homeostasis. Both differential tissue composition and gene enrichment analyses pointed to an enrichment of infiltrating immune cell types within the tissue as the predominant cause of this difference. Monocytes and macrophages had the greatest presence within the periprostatic adipose tissue, compared with other immune cells. The abundance of these immune cell types was positively associated with androgen deprivation, suggesting their infiltration of the tissue, which is consistent with *in vivo* studies (57). Macrophages have been shown to interact with adipose tissue in a paracrine manner, where TNF-α secretion from macrophages interferes with adipocyte insulin signalling and induces fatty acid lipolysis, which commences a vicious inflammatory cycle and contributes to insulin resistance (58). Furthermore, an elevated blood monocyte count is an independent prognostic predictor for poor prostate cancer outcome in cancer-specific and overall survival studies (59, 60). These finding are perhaps not surprising, given numerous reports describing the anti-inflammatory properties of androgen receptor signalling. How this is mediated is not clear, although testosterone has been reported to attenuate both Th2 and Th17 inflammatory responses (61, 62), as well as directly suppressing the section of monocyte chemoattractant protein-1 in adipocytes, a key cytokine that promotes monocyte infiltration (63).

There are a number of limitations to our study that merit enumeration, particularly the lack of orthogonal validation at the protein level for pathway and/or cell type tissue enrichment observed in our expression profiles. However, we note that previous studies have confirmed that alterations of inflammatory signalling identified expression data are accurately reflected by protein level changes in the abundance of key cytokines, including IL6 (64), and extensive validation studies have shown that the expression of key inflammatory cell markers are consistent with expression data from RNA-seq analysis (65) (www.proteinatlas.org). In addition, ideally we would use paired pre- and post-treatment samples from the same patients for analysis. However, this was not practical for clinical reasons, as collection of sufficient quantities of periprostatic adipose tissue for the type of exploratory analysis described is only possible at the time of prostatectomy. We have therefore tried to match patients as much as possible based on their pre-treatment clinical and pathological characteristics as described.

Taken together, our study demonstrates that androgen deprivation promotes an inflammatory and obesity-like microenvironment in periprostatic fat and suggests that the beneficial effect of ADT may be partially counteracted by metabolic and inflammatory side effects in the adipose tissue encompassing the prostate. This may be particular pertinent when the primary tumour is *in situ*, as tumour response within the prostate appears less profound compared to that observed for metastatic disease (66, 67). Further studies will need to investigate the immune infiltration profile associated with androgen deprivation, as well as the potential impact of anti-inflammatory therapies on local tumour response.

Online methods and raw data

The code used to conduct the analyses is available at https://github.com/stemangiola/ADT_fat. The sequenced reads raw files are available at https://ega-archive.org/ with the identifier EGAD00001004971.

Supplementary data
This is linked to the online version of the paper at https://doi.org/10.1530/EC-19-0029.

Declaration of interest
The authors declare that there is no conflict of interest that could be perceived as prejudicing the impartiality of the research reported.

Funding
Stefano Mangiola is supported by the David Mayor PhD Scholarship from the Prostate Cancer Research Foundation. Ken Chow is supported by a Postgraduate Medical Research Scholarship from the Prostate Cancer Research Fund and the Australian Government Research Training Program Scholarship provided by the Australian Commonwealth Government and the University of Melbourne. Niall M Corcoran is supported by a David Bickart Clinician Research Fellowship from the Faculty of Medicine, Dentistry and Health Sciences at the University of Melbourne, as well a Movember – Distinguished Gentleman's Ride Clinician Scientist Award through Prostate Cancer Foundation of Australia's Research Programme. Sample analysis was funded through a Victorian Cancer Agency Early Career Seed Grant to N M C (ECSG14010).

Acknowledgements
The authors acknowledge all the patients who participated in the study as well the surgeons involved in tissue collection.

References

1 Huggins C, Stevens RE & Hodges CV. Studies on prostatic cancer: the effects of castration on advanced carcinoma of the prostate gland. *Archives of Surgery* 1941 **43** 209–223. (https://doi.org/10.1001/archsurg.1941.01210140043004)
2 James ND, Spears MR, Clarke NW, Dearnaley DP, De Bono JS, Gale J, Hetherington J, Hoskin PJ, Jones RJ, Laing R, *et al*. Survival with

newly diagnosed metastatic prostate cancer in the 'docetaxel era': data from 917 patients in the control arm of the STAMPEDE trial (mrc pr08, cruk/06/019). *European Urology* 2015 **67** 1028–1038. (https://doi.org/10.1016/j.eururo.2014.09.032)

3 Rhee H, Gunter JH, Heathcote P, Ho K, Stricker P, Corcoran NM & Nelson CC. Adverse effects of androgen-deprivation therapy in prostate cancer and their management. *BJU International* 2015 **115** (Supplement 5) 3–13. (https://doi.org/10.1111/bju.12964)

4 Faris JE & Smith MR. Metabolic sequelae associated with androgen deprivation therapy for prostate cancer. *Current Opinion in Endocrinology, Diabetes, and Obesity* 2010 **17** 240–246. (https://doi.org/10.1097/MED.0b013e3283391fd1)

5 Braunstein LZ, Chen MH, Loffredo M, Kantoff PW & D'Amico AV. Obesity and the odds of weight gain following androgen deprivation therapy for prostate cancer. *Prostate Cancer* 2014 **2014** 230812. (https://doi.org/10.1155/2014/230812)

6 Comitato R, Saba A, Turrini A, Arganini C & Virgili F. Sex hormones and macronutrient metabolism. *Critical Reviews in Food Science and Nutrition* 2015 **55** 227–241. (https://doi.org/10.1080/10408398.2011.651177)

7 van Londen GJ, Levy ME, Perera S, Nelson JB & Greenspan SL. Body composition changes during androgen deprivation therapy for prostate cancer: a 2-year prospective study. *Critical Reviews in Oncology/Hematology* 2008 **68** 172–177. (https://doi.org/10.1016/j.critrevonc.2008.06.006)

8 Dockery F, Bulpitt CJ, Agarwal S, Donaldson M & Rajkumar C. Testosterone suppression in men with prostate cancer leads to an increase in arterial stiffness and hyperinsulinaemia. *Clinical Science* 2003 **104** 195–201. (https://doi.org/10.1042/CS20020209)

9 Smith JC, Bennett S, Evans LM, Kynaston HG, Parmar M, Mason MD, Cockcroft JR, Scanlon MF & Davies JS. The effects of induced hypogonadism on arterial stiffness, body composition, and metabolic parameters in males with prostate cancer. *Journal of Clinical Endocrinology and Metabolism* 2001 **86** 4261–4267. (https://doi.org/10.1210/jcem.86.9.7851)

10 Smith MR, Lee H & Nathan DM. Insulin sensitivity during combined androgen blockade for prostate cancer. *Journal of Clinical Endocrinology and Metabolism* 2006 **91** 1305–1308. (https://doi.org/10.1210/jc.2005-2507)

11 Chow K, Mangiola S, Vazirani J, Peters JS, Costello AJ, Hovens CM & Corcoran NM. Obesity suppresses tumor attributable psa, affecting risk categorization. *Endocrine-Related Cancer* 2018 **25** 561–568. (https://doi.org/10.1530/ERC-17-0466)

12 Freedland SJ & Aronson WJ. Examining the relationship between obesity and prostate cancer. *Reviews in Urology* 2004 **6** 73–81.

13 Freedland SJ, Aronson WJ, Kane CJ, Presti JC, Jr, Amling CL, Elashoff D & Terris MK. Impact of obesity on biochemical control after radical prostatectomy for clinically localized prostate cancer: a report by the shared equal access regional cancer hospital database study group. *Journal of Clinical Oncology* 2004 **22** 446–453. (https://doi.org/10.1200/JCO.2004.04.181)

14 Amling CL, Kane CJ, Riffenburgh RH, Ward JF, Roberts JL, Lance RS, Friedrichs PA & Moul JW. Relationship between obesity and race in predicting adverse pathologic variables in patients undergoing radical prostatectomy. *Urology* 2001 **58** 723–728. (https://doi.org/10.1016/S0090-4295(01)01373-5)

15 Mydlo JH, Tieng NL, Volpe MA, Chaiken R & Kral JG. A pilot study analyzing psa, serum testosterone, lipid profile, body mass index and race in a small sample of patients with and without carcinoma of the prostate. *Prostate Cancer and Prostatic Diseases* 2001 **4** 101–105. (https://doi.org/10.1038/sj.pcan.4500514)

16 Rohrmann S, Roberts WW, Walsh PC & Platz EA. Family history of prostate cancer and obesity in relation to high-grade disease and extraprostatic extension in young men with prostate cancer. *Prostate* 2003 **55** 140–146. (https://doi.org/10.1002/pros.10211)

17 Amling CL, Riffenburgh RH, Sun L, Moul JW, Lance RS, Kusuda L, Sexton WJ, Soderdahl DW, Donahue TF, Foley JP, *et al*. Pathologic variables and recurrence rates as related to obesity and race in men with prostate cancer undergoing radical prostatectomy. *Journal of Clinical Oncology* 2004 **22** 439–445. (https://doi.org/10.1200/JCO.2004.03.132)

18 Andersson SO, Wolk A, Bergström R, Adami HO, Engholm G, Englund A & Nyrén O. Body size and prostate cancer: a 20-year follow-up study among 135006 Swedish construction workers. *Journal of the National Cancer Institute* 1997 **89** 385–389. (https://doi.org/10.1093/jnci/89.5.385)

19 Calle EE, Rodriguez C, Walker-Thurmond K & Thun MJ. Overweight, obesity, and mortality from cancer in a prospectively studied cohort of U.S. adults. *New England Journal of Medicine* 2003 **348** 1625–1638. (https://doi.org/10.1056/NEJMoa021423)

20 Rodriguez C, Patel AV, Calle EE, Jacobs EJ, Chao A & Thun MJ. Body mass index, height, and prostate cancer mortality in two large cohorts of adult men in the united states. *Cancer Epidemiology, Biomarkers and Prevention* 2001 **10** 345–353.

21 Snowdon DA, Phillips RL & Choi W. Diet, obesity, and risk of fatal prostate cancer. *American Journal of Epidemiology* 1984 **120** 244–250. (https://doi.org/10.1093/oxfordjournals.aje.a113886)

22 Mangiola S, Stuchbery R, Macintyre G, Clarkson MJ, Peters JS, Costello AJ, Hovens CM & Corcoran NM. Periprostatic fat tissue transcriptome reveals a signature diagnostic for high-risk prostate cancer. *Endocrine-Related Cancer* 2018 **25** 569–581. (https://doi.org/10.1530/ERC-18-0058)

23 Kerger M, Hong MKH, Pedersen J, Nottle T, Ryan A, Mills J, Peters JS, Moon D, Crowe H, Costello AJ, *et al*. Microscopic assessment of fresh prostate tumour specimens yields significantly increased rates of correctly annotated samples for downstream analysis. *Pathology* 2012 **44** 204–208. (https://doi.org/10.1097/PAT.0b013e3283511c96)

24 Cooperberg MR, Broering JM & Carroll PR. Risk assessment for prostate cancer metastasis and mortality at the time of diagnosis. *Journal of the National Cancer Institute* 2009 **101** 878–887. (https://doi.org/10.1093/jnci/djp122)

25 Andrews S. FastQC: a quality control tool for high throughput sequence data. Cambridge, UK: Babraham Bioinformatics, 2010. (available at: https://www.bioinformatics.babraham.ac.uk/projects/fastqc/)

26 Bolger AM, Lohse M & Usadel B. Trimmomatic: a flexible trimmer for Illumina sequence data. *Bioinformatics* 2014 **30** 2114–2120. (https://doi.org/10.1093/bioinformatics/btu170)

27 Dobin A, Davis CA, Schlesinger F, Drenkow J, Zaleski C, Jha S, Batut P, Chaisson M & Gingeras TR. Star: ultrafast universal rna-seq aligner. *Bioinformatics* 2013 **29** 15–21. (https://doi.org/10.1093/bioinformatics/bts635)

28 Liao Y, Smyth GK & Shi W. Featurecounts: an efficient general purpose program for assigning sequence reads to genomic features. *Bioinformatics* 2014 **30** 923–930. (https://doi.org/10.1093/bioinformatics/btt656)

29 Risso D, Ngai J, Speed TP & Dudoit S. Normalization of RNA-seq data using factor analysis of control genes or samples. *Nature Biotechnology* 2014 **32** 896–902. (https://doi.org/10.1038/nbt.2931)

30 Robinson MD, McCarthy DJ & Smyth GK. Edger: a bioconductor package for differential expression analysis of digital gene expression data. *Bioinformatics* 2010 **26** 139–140. (https://doi.org/10.1093/bioinformatics/btp616)

31 Alhamdoosh M, Ng M, Wilson N, Sheridan J, Huynh H, Wilson M & Ritchie ME. Combining multiple tools outperforms individual methods in gene set enrichment analyses. *Bioinformatics* 2017 **33** btw623. (http://doi.org/10.1093/bioinformatics/btw623)

32 Subramanian A, Tamayo P, Mootha VK, Mukherjee S, Ebert BL, Gillette MA, Paulovich A, Pomeroy SL, Golub TR, Lander ES, *et al*. Gene set enrichment analysis: a knowledge-based approach for

interpreting genome-wide expression profiles. *PNAS* 2005 **102** 15545–15550. (https://doi.org/10.1073/pnas.0506580102)

33 Newman AM, Liu CL, Green MR, Gentles AJ, Feng W, Xu Y, Hoang CD, Diehn M & Alizadeh AA. Robust enumeration of cell subsets from tissue expression profiles. *Nature Methods* 2015 **12** 453–457. (https://doi.org/10.1038/nmeth.3337)

34 Maier MJ. DirichletReg: Dirichlet regression for compositional data in R. In *Research Report Series / Department of Statistics and Mathematics*. Vienna, Austria: WU Vienna University of Economics and Business, 2014. (available at: http://epub.wu.ac.at/4077/)

35 Carpenter B, Gelman A, Hoffman M, Lee D, Goodrich B, Betancourt M, Brubaker MA, Guo J, Li P, Riddell A, *et al*. Stan: a probabilistic programming language. *Journal of Statistical Software* 2016 **20** 1–37.

36 Corcoran NM, Hong MKH, Casey RG, Hurtado-Coll A, Peters J, Harewood L, Goldenberg SL, Hovens CM, Costello AJ & Gleave ME. Upgrade in Gleason score between prostate biopsies and pathology following radical prostatectomy significantly impacts upon the risk of biochemical recurrence. *BJU International* 2011 **108** E202–E210. (https://doi.org/10.1111/j.1464-410X.2011.10119.x)

37 Corcoran NM, Hovens CM, Hong MKH, Pedersen J, Casey RG, Connolly S, Peters J, Harewood L, Gleave ME, Goldenberg SL, *et al*. Underestimation of Gleason score at prostate biopsy reflects sampling error in lower volume tumours. *BJU International* 2012 **109** 660–664. (https://doi.org/10.1111/j.1464-410X.2011.10543.x)

38 Ritchie ME, Phipson B, Wu D, Hu Y, Law CW, Shi W & Smyth GK. Limma powers differential expression analyses for rna-sequencing and microarray studies. *Nucleic Acids Research* 2015 **43** e47. (https://doi.org/10.1093/nar/gkv007)

39 Ashburner M, Ball CA, Blake JA, Botstein D, Butler H, Cherry JM, Davis AP, Dolinski K, Dwight SS, Eppig JT, *et al*. Gene ontology: tool for the unification of biology. *Nature Genetics* 2000 **25** 25–29. (https://doi.org/10.1038/75556)

40 Nebert DW & Russell DW. Clinical importance of the cytochromes p450. *Lancet* 2002 **360** 1155–1162. (https://doi.org/10.1016/S0140-6736(02)11203-7)

41 Sampath H & Ntambi JM. The role of fatty acid desaturases in epidermal metabolism. *Dermato-Endocrinology* 2011 **3** 62–64. (https://doi.org/10.4161/derm.3.2.14832)

42 Bianco AC & Kim BW. Deiodinases: implications of the local control of thyroid hormone action. *Journal of Clinical Investigation* 2006 **116** 2571–2579. (https://doi.org/10.1172/JCI29812)

43 Panigrahi SK, Manterola M & Wolgemuth DJ. Meiotic failure in cyclin a1-deficient mouse spermatocytes triggers apoptosis through intrinsic and extrinsic signaling pathways and 14-3-3 proteins. *PLoS ONE* 2017 **12** e0173926. (https://doi.org/10.1371/journal.pone.0173926)

44 Lefranc M-P. Immunoglobulin and T cell receptor genes: Imgt® and the birth and rise of immunoinformatics. *Frontiers in Immunology* 2014 **5** 22. (https://doi.org/10.3389/fimmu.2014.00022)

45 Ressler SJ, Dang TD, Wu SM, Tse DY, Gilbert BE, Vyakarnam A, Yang F, Schauer IG, Barron DA & Rowley DR. Wfdc1 is a key modulator of inflammatory and wound repair responses. *American Journal of Pathology* 2014 **184** 2951–2964. (https://doi.org/10.1016/j.ajpath.2014.07.013)

46 Das SK, Ma L & Sharma NK. Adipose tissue gene expression and metabolic health of obese adults. *International Journal of Obesity* 2015 **39** 869–873. (https://doi.org/10.1038/ijo.2014.210)

47 Jones RJ, Dickerson S, Bhende PM, Delecluse HJ & Kenney SC. Epstein-Barr virus lytic infection induces retinoic acid-responsive genes through induction of a retinol-metabolizing enzyme, dhrs9. *Journal of Biological Chemistry* 2007 **282** 8317–8324. (https://doi.org/10.1074/jbc.M608667200)

48 Riquelme P, Amodio G, Macedo C, Moreau A, Obermajer N, Brochhausen C, Ahrens N, Kekarainen T, Fändrich F, Cuturi C, *et al*. Dhrs9 is a stable marker of human regulatory macrophages. *Transplantation* 2017 **101** 2731–2738. (https://doi.org/10.1097/TP.0000000000001814)

49 Xiang J, Guo R, Wan C, Wu L, Yang S & Guo D. Regulation of intestinal epithelial calcium transport proteins by stanniocalcin-1 in $CaCO_2$ cells. *International Journal of Molecular Sciences* 2016 **17** E1095. (https://doi.org/10.3390/ijms17071095)

50 Kapoor J, Namdarian B, Pedersen J, Hovens C, Moon D, Peters J, Costello AJ, Ruljancich P & Corcoran NM. Extraprostatic extension into periprostatic fat is a more important determinant of prostate cancer recurrence than an invasive phenotype. *Journal of Urology* 2013 **190** 2061–2066. (https://doi.org/10.1016/j.juro.2013.06.050)

51 Ribeiro R, Monteiro C, Cunha V, Oliveira MJ, Freitas M, Fraga A, Príncipe P, Lobato C, Lobo F, Morais A, *et al*. Human periprostatic adipose tissue promotes prostate cancer aggressiveness in vitro. *Journal of Experimental and Clinical Cancer Research* 2012 **31** 32. (https://doi.org/10.1186/1756-9966-31-32)

52 Ribeiro RJT, Monteiro CPD, Cunha VFPM, Azevedo ASM, Oliveira MJ, Monteiro R, Fraga AM, Príncipe P, Lobato C, Lobo F, *et al*. Tumor cell-educated periprostatic adipose tissue acquires an aggressive cancer-promoting secretory profile. *Cellular Physiology and Biochemistry* 2012 **29** 233–240. (https://doi.org/10.1159/000337604)

53 Finley DS, Calvert VS, Inokuchi J, Lau A, Narula N, Petricoin EF, Zaldivar F, Santos R, Tyson DR & Ornstein DK. Periprostatic adipose tissue as a modulator of prostate cancer aggressiveness. *Journal of Urology* 2009 **182** 1621–1627. (https://doi.org/10.1016/j.juro.2009.06.015)

54 Buschemeyer WC, 3rd & Freedland SJ. Obesity and prostate cancer: epidemiology and clinical implications. *European Urology* 2007 **52** 331–343. (https://doi.org/10.1016/j.eururo.2007.04.069)

55 Baumgartner RN. Body composition in healthy aging. *Annals of the New York Academy of Sciences* 2000 **904** 437–448. (https://doi.org/10.1111/j.1749-6632.2000.tb06498.x)

56 Stenholm S, Harris TB, Rantanen T, Visser M, Kritchevsky SB & Ferrucci L. Sarcopenic obesity: definition, cause and consequences. *Current Opinion in Clinical Nutrition and Metabolic Care* 2008 **11** 693–700. (https://doi.org/10.1097/MCO.0b013e328312c37d)

57 Oh DY, Morinaga H, Talukdar S, Bae EJ & Olefsky JM. Increased macrophage migration into adipose tissue in obese mice. *Diabetes* 2012 **61** 346–354. (https://doi.org/10.2337/db11-0860)

58 Suganami T, Nishida J & Ogawa Y. A paracrine loop between adipocytes and macrophages aggravates inflammatory changes: role of free fatty acids and tumor necrosis factor alpha. *Arteriosclerosis, Thrombosis, and Vascular Biology* 2005 **25** 2062–2068. (https://doi.org/10.1161/01.ATV.0000183883.72263.13)

59 Nonomura N, Takayama H, Nakayama M, Nakai Y, Kawashima A, Mukai M, Nagahara A, Aozasa K & Tsujimura A. Infiltration of tumour-associated macrophages in prostate biopsy specimens is predictive of disease progression after hormonal therapy for prostate cancer. *BJU International* 2011 **107** 1918–1922. (https://doi.org/10.1111/j.1464-410X.2010.09804.x)

60 Wang YQ, Zhu YJ, Pan JH, Xu F, Shao XG, Sha JJ, Liu Q, Huang YR, Dong BJ & Xue W. Peripheral monocyte count: an independent diagnostic and prognostic biomarker for prostate cancer – a large Chinese cohort study. *Asian Journal of Andrology* 2017 **19** 579–585. (https://doi.org/10.4103/1008-682X.186185)

61 Fuseini H, Yung JA, Cephus JY, Zhang J, Goleniewska K, Polosukhin VV, Peebles RS, Jr & Newcomb DC. Testosterone decreases house dust mite-induced type 2 and il-17a-mediated airway inflammation. *Journal of Immunology* 2018 **201** 1843–1854. (https://doi.org/10.4049/jimmunol.1800293)

62 Laffont S, Blanquart E, Savignac M, Cénac C, Laverny G, Metzger D, Girard JP, Belz GT, Pelletier L, Seillet C, *et al*. Androgen signaling negatively controls group 2 innate lymphoid cells. *Journal of Experimental Medicine* 2017 **214** 1581–1592. (https://doi.org/10.1084/jem.20161807)

63 Morooka N, Ueguri K, Yee KKL, Yanase T & Sato T. Androgen-androgen receptor system improves chronic inflammatory conditions by suppressing monocyte chemoattractant protein-1 gene expression in adipocytes via transcriptional regulation. *Biochemical and Biophysical Research Communications* 2016 **477** 895–901. (https://doi.org/10.1016/j.bbrc.2016.06.155)

64 Katsura A, Tamura Y, Hokari S, Harada M, Morikawa M, Sakurai T, Takahashi K, Mizutani A, Nishida J, Yokoyama Y, *et al*. Zeb1-regulated inflammatory phenotype in breast cancer cells. *Molecular Oncology* 2017 **11** 1241–1262. (https://doi.org/10.1002/1878-0261.12098)

65 Uhlén M, Fagerberg L, Hallström BM, Lindskog C, Oksvold P, Mardinoglu A, Sivertsson Å, Kampf C, Sjöstedt E, Asplund A, *et al*. Proteomics. Tissue-based map of the human proteome. *Science* 2015 **347** 1260419. (https://doi.org/10.1126/science.1260419)

66 Montgomery B, Tretiakova MS, Joshua AM, Gleave ME, Fleshner N, Bubley GJ, Mostaghel EA, Chi KN, Lin DW, Sanda M, *et al*. Neoadjuvant enzalutamide prior to prostatectomy. *Clinical Cancer Research* 2017 **23** 2169–2176. (https://doi.org/10.1158/1078-0432.CCR-16-1357)

67 Tombal B, Borre M, Rathenborg P, Werbrouck P, Van Poppel H, Heidenreich A, Iversen P, Braeckman J, Heracek J, Baskin-Bey E, *et al*. Enzalutamide monotherapy in hormone-naive prostate cancer: primary analysis of an open-label, single-arm, phase 2 study. *Lancet: Oncology* 2014 **15** 592–600. (https://doi.org/10.1016/S1470-2045(14)70129-9)

Received in final form 14 March 2019
Accepted 4 April 2019
Accepted Preprint published online 4 April 2019